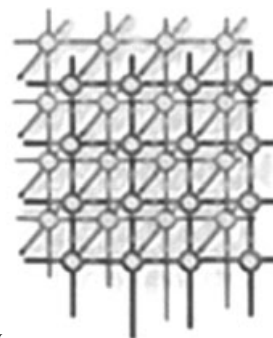


Pattern informatics approach to earthquake forecasting in 3D



Y. Toya^{1,*},†, K. F. Tiampo¹, J. B. Rundle², Chien-chih Chen³, Hsien-Chi Li³ and W. Klein⁴

¹*Department of Earth Sciences, University of Western Ontario, London, ON, Canada*

²*Department of Physics and Geology, University of California, Davis, CA, U.S.A.*

³*Earth Sciences and Grad. Inst. Geophysics, National Central University, Zhongli, Taiwan 320, Taiwan*

⁴*Department of Physics, Boston University, Boston, MA, U.S.A.*

SUMMARY

Natural seismicity is correlated across multiple spatial and temporal scales, but correlations in seismicity prior to a large earthquake are locally subtle (e.g. seismic quiescence) and often prominent in broad scale (e.g. seismic activation), resulting in local and regional seismicity patterns, e.g. a Mogi's donut. Recognizing that patterns in seismicity rate are reflecting the regional dynamics of the directly unobservable crustal stresses, the Pattern Informatics (PI) approach was introduced by Tiampo *et al.* and Rundle *et al.* in 2002. In this study, we expand the PI approach to forecasting earthquakes into the third or vertical dimension, and illustrate its further improvement in the forecasting performance through case studies of both natural and synthetic data. The PI characterizes rapidly evolving spatio-temporal seismicity patterns as angular drifts of a unit state vector in a high-dimensional correlation space, and systematically identifies anomalous shifts in seismic activity with respect to the regional background. 3D PI analysis is particularly advantageous over 2D analysis in resolving vertically overlapped seismicity anomalies in a highly complex tectonic environment. Case studies will help to illustrate some important properties of the PI forecasting tool. Copyright © 2009 John Wiley & Sons, Ltd.

Received 31 October 2008; Accepted 24 July 2009

KEY WORDS: pattern informatics; effective ergodicity; earthquake forecasting; seismicity rate

*Correspondence to: Y. Toya, Department of Earth Sciences, University of Western Ontario, London, ON, Canada.

†E-mail: ytoya@uwo.ca; yuzo.toya@gmail.com

Contract/grant sponsor: NSERC

Contract/grant sponsor: Aon Benfield/ICLR IRC

Contract/grant sponsor: SCEC; contract/grant number: 1243

Contract/grant sponsor: NSF Cooperative Agreement; contract/grant number: EAR-0529922

Contract/grant sponsor: USGS Cooperative Agreement; contract/grant number: 07HQAG0008



1. INTRODUCTION

Earthquake forecasting and fault zone characterization for earthquake hazard analysis are some of the important goals of earthquake studies. Acquisition of quality earthquake data and refinement of analysis techniques make these aims increasingly feasible. A promising intermediate-term earthquake forecasting PI method [1–4] is based on phase dynamics concept from statistical mechanics, which provides a macroscopic portrait of complex microscale physical processes [5] in terms of both threshold dynamics and long-range interactions of these microscale faults [1–4, 6–8]. In this view, the highly correlated space–time dynamics of small to moderate magnitude seismicity, driven by a steady loading of the regional stress, can be characterized by the rotations of a time-dependent unit state vector in a real-valued Hilbert space about the origin. Our interest lies solely in the space–time fluctuations or rotations of this phase angle, i.e. the phase dynamics concept [9]. Non-random and persistent rotation of this phase angle provides information on the trend of correlated seismicity anomalies in the system under investigation, measured with respect to the nearly stationary background [1–4]. A 2D version of this method has been shown to work effectively in forecasting moderate to large natural earthquakes in various parts of the world including California, Japan, Taiwan, and Canada [10–16]. Here, the method is being developed for 3D applications in a variety of tectonic environments, including the subduction zone setting, and the properties of the PI approach will be illustrated through case studies of both synthetic and natural seismicity data.

2. METHOD

2.1. Data quality

Event location accuracy, earthquake catalog homogeneity, and magnitude of completeness are important aspects of seismicity rate studies, in order to detect the real or natural changes in the seismicity rate. Catalog homogeneity and completeness can, for instance, be disrupted by some artificial changes in observational station coverage [17–19], large earthquake occurrences, where catalog incompleteness can result directly from the masking effect on small events from relatively large sequences of aftershocks near the main events, in addition to the incomplete collection of small events in some regions [20]. In order to resolve these issues we take the following measures: (i) Select the quality catalogs and include multiple catalogs in the analysis, where such data are available, in order to evaluate the consistency of analysis results (e.g. [21]); (ii) Perform independent evaluations of the catalog homogeneity (e.g. [17–19]), the magnitude of completeness (e.g. [22–24]), and the validity of the assumption of effective ergodicity on each fault system under investigation (e.g. [25,26]); and (iii) Perform a comparison of the PI analysis results and one formulation of the optimal forecasting approach (cf. [12], [27–31]).

In order to perform (i), above, we choose for the analysis instrumentally recorded earthquake data: from the Centennial Earthquake Catalog (Centennial) [32,33] and the Advanced National Seismic System (ANSS) catalog [34] for the retrospective analysis of seismicity in Sumatra region; the Central Weather Bureau Seismic Network (CWB) catalog for a study in Taiwan region; and the National Earthquake Database of Canada (NRC) [35] for a study in western Canada. The Centennial composite catalog, prepared by Engdahl and Villaseñor [32] with the aim to compile



a homogeneous catalog of global seismicity in the 20th century, contains relocated hypocenter data [33] and a complete listing of events with $M \geq 5.5$ since 1964 in their preferred or adjusted magnitude scale [32]. The ANSS composite catalog and the other catalogs used in the analysis, on the other hand, are carefully evaluated for catalog homogeneity in our specific study areas.

Each earthquake catalog is examined with special attention given to catalog homogeneity and completeness, the presence/non-presence of large event sequences with numerous dependent after-shocks, and the reported seismicity depths. We do not apply any artificial declustering with arbitrary windowing algorithms on the data prior to a PI analysis, as the nature of clustering or anti-clustering phenomena present in the data is a part of what we seek to study in the analysis. Effects of artificial declustering on PI analysis performance will be discussed elsewhere.

Earthquake catalog often contains default depth information that is routinely assigned by seismic networks for those inadequately located events. This requires the use of some precautions as it relates to the definition of observational parameters and the interpretation of analysis results in 3D. Nonetheless, the PI index is robust and largely insensitive to the incompleteness of event records so long as the cataloging is performed consistently or homogeneously.

PI analysis assumes that the regional background seismicity rate of a given fault system under investigation is stationary. This is a necessary condition for the best performance of the PI, which utilizes a linear operator in its calculation [1–4,7]. In addition, stationarity is necessary, although not sufficient, condition, for physical processes to be ergodic (e.g. [25,26]). When statistically ergodic periods and parameter ranges are selected for a particular PI analysis, its forecasting power should improve [15]. Accordingly, we make an effort to validate this assumption by analyzing the effective ergodicity of the fault system under investigation using the well-known Thirumalai and Mountain (TM) metric (e.g. [36]).

TM metric $\Omega_e(t)$ is defined as:

$$\Omega_e(t) = \frac{1}{N} \sum_{i=1}^N [\varepsilon_i(t) - \bar{\varepsilon}(t)]^2 \quad (1)$$

$$\bar{\varepsilon}(t) = \frac{1}{N} \sum_{i=1}^N \varepsilon_i(t) \quad (2)$$

$$\varepsilon_i(t) = \frac{1}{t} \int_0^t E_i(t') dt' \quad (3)$$

where $E_i(t')$ is the value of the energy in i th cell at time t' , which is assumed to be equal to the number of earthquakes of a given minimum magnitude or larger in a catalog at time t' [26]; $\varepsilon_i(t)$ is the time-averaged rate of seismicity in i th cell or element of N discretized cells in a system; $\bar{\varepsilon}(t)$ is the ensemble average of N temporal averages in the system; and $\Omega_e(t)$ is the TM metric or fluctuation metric, which is essentially the spatial variance of N temporal averages over the study area for a given time-interval t . This metric is calculated at every successive time step, and is used to evaluate whether the phase space is explored equally with time [26]. In an effectively ergodic system, temporal and spatial activities of individual elements in the system would be practically indistinguishable in terms of its averaged properties [36]. Such a state is said to be in statistical equilibrium [26] and the inverse of the metric has a linear relationship with increasing time-interval t



[8,25,26,36,37]. A detailed discussion on the application of TM metric to seismicity studies is found in Tiampo *et al.* [26]. Plots of the inverse TM metric versus time show linearly increasing values of the inverse metric for those time periods where the system is effectively ergodic, or the spatial and temporal averages approach the same constant values.

TM metric is very sensitive to changes in seismicity rate, and the linearity of inverse TM curves will break in response to various types of rate changes in the system. These include gradual detection level increases in a seismic network or a sequence of large earthquakes with numerous aftershocks, etc. [26]. The TM metric is more sensitive than the algorithm developed by Habermann [17], used to detect systematic rate changes or breaks in the temporal stationarity of seismic activity apparent in a catalog. In addition, the TM metric can detect obscure (spatio-temporal) rate changes in seemingly stationarity processes.

2.2. Pattern Informatics (PI) index

The PI method applied here in 3D is, in essence, identical to the original method [1,2,10,11,15,16]. The linear decomposition of synthetic seismicity from a numerical fault model of California and its reconstruction were originally introduced by Rundle *et al.* [3], and expanded for the investigations of natural seismicity in [1,2,4,7]. It is based on the idea that both fault movements and seismicity are good proxies for directly unobservable stress fluctuations (e.g. [38,39]). The PI method quantifies local and regional stress interactions in a fault system through the objective characterization of seismicity rate changes. Further details can be found in Tiampo *et al.* [1,2,10,11,16].

The calculation of the PI index takes six basic steps as described in Table I. The details of further modified versions of the original method [1,2,10,11,16] are found in Holliday and coworkers [12–14,16,28–31].

First, a study area is discretized into N cells of dimensions: ‘ dX ’ in longitude by ‘ dX ’ in latitude by ‘ dZ ’ in depth {Step 1}. Next, the time-average rate of earthquakes ($M \geq M_{\min}$), $\psi_{obs}(x_i, t)$, is individually calculated in each cell ‘ i ’ for time periods: $[t_0, t_1)$ and $[t_0, t_2)$, to construct seismicity rate functions:

$$S(x_i, t_0, t) = \frac{1}{(t - t_0)} \int_{t_0}^t \psi_{obs}(x_i, t) dt \quad (4)$$

Table I. The PI method (Flow chart).

Step 1:	Discretization of a study area into N cells (Each cell is dX by dX by dZ in size.)
Step 2:	Calculate activity rate $\psi_{obs}(x_i, t)$ and construct seismicity function $S(x_i, t_0, t)$ for each cell (x_i)
Step 3:	Construct the phase function $S'(x_i, t_0, t)$ (See text.)
Step 4:	Calculate the important changes in seismicity or the rotation of the N -dimensional unit vector: $\Delta S'(x_i, t_1, t_2) = S'(x_i, t_0, t_2) - S'(x_i, t_0, t_1)$
Step 5:	De-noising and removal of the free parameter, the choice of base year
Step 6:	Relate probabilities to the square of the associated vector phase function



where $t = t_1$ or t_2 {Step 2}. Then, the mean-zero unit-norm phase function $S'(x_i, t_0, t)$ for $t = t_1$ or t_2 is calculated as

$$S'(x_i, t_0, t) = \frac{S(x_i, t_0, t) - \langle S(x_i, t_0, t) \rangle}{\|S(x_i, t_0, t)\|} \tag{5}$$

where $\langle S(x_i, t_0, t) \rangle$ is the spatial mean and $\|S(x_i, t_0, t)\|$ is the standard error of N spatially distributed S functions in the study area {Step 3}.

The important rotation of the N -dimensional unit state vector is, then, calculated in {Step 4}:

$$\Delta S' = S'(x_i, t_b, t_2) - S'(x_i, t_b, t_1) \tag{6}$$

To identify the coherent trends in $\Delta S'$ and to practically remove the choice of a free parameter, base year (t_b) is varied along the time-axis for all possible values in the range of $[t_0, t_2)$ and the representative values of $\Delta S'$ are obtained by averaging them in time {Step 5}.

The idea here is that the shift in the earthquake activity rate from one state t_1 to another t_2 can be characterized by this rotation $\Delta S'(x_i, t_1, t_2)$ of the state vector S'_i [1,2]. We are solely interested in this angular drift $\Delta S'$, and the $L2$ -norm of the state vector is assumed to be constant. Again, delineation of the effectively ergodic regions of the associated parameter space helps to ensure that this is true for the period of time under evaluation. As we look for the probability increase beyond the background mean amplitude, we compute $\Delta P(x_i, t_1, t_2)$ or the anomalous change in probability of an event, the PI index, as follows:

$$\Delta P(x_i, t_1, t_2) = \{\Delta S'(x_i, t_1, t_2)\}^2 - \mu \tag{7}$$

where μ is the spatial mean of $\{\Delta S'(x_i, t_1, t_2)\}^2$.

The PI method has been applied to various seismically active regions of the world, e.g. California, Taiwan, Japan, and others (e.g. [1,2,10–16,28–31,40]), and shown to successfully forecast moderate magnitude earthquakes, given a good quality earthquake catalog of small magnitude events. The technique is also capable of identifying both activation and quiescence anomalies in seismicity patterns [1,2] (Table II; Figures 1–4).

2.3. Mapping parameters

The horizontal dimension of a discretization cell (dX) and the vertical cell size (dZ) for a 3D analysis are typically selected to match the linear dimension of a target event to be forecast. These values can be set based upon the estimates of typical surface rupture length and width dimensions [1,2] or by following an empirical relation such as that of Wells and Coppersmith [12,41]. Ideally, however, the optimal discretization cell dimension should be defined so as to maximize the forecasting performance even with the presence of significant spatial clustering in data (aftershocks of large earthquakes), which may not be representative of a statistically independent sample in the point process of interest. A grid search would systematically help us to select the appropriate discretization dimension so as to minimize the potential effects from ergodicity breaking clustering in data, given a set of map boundary or ensemble size [cf. 15,16,31,42]. Furthermore, automatic grid search would be a practical approach, when we have not yet accumulated the empirical information regarding the relationship between the linear dimensions of target events and PI index anomalies.

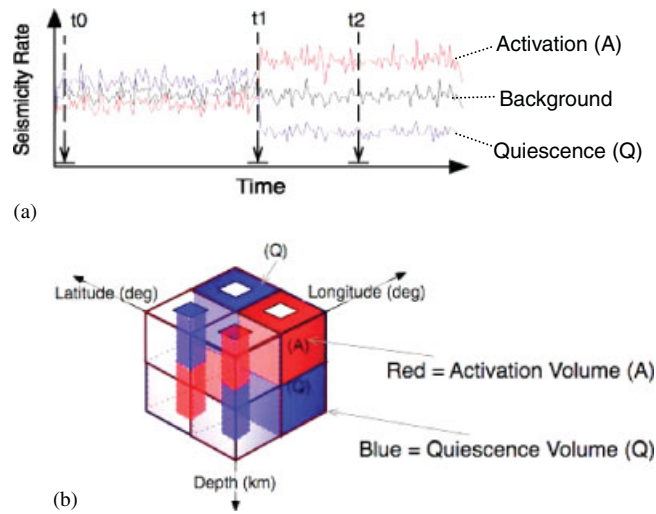


Figure 1. Synthetic uniform random event catalog with rate changes given at known instances: (a) in time and (b) in space. (Also, (b) illustrates the expected or ideal distribution of $\Delta S'$ anomalies in 3D PI analysis.)

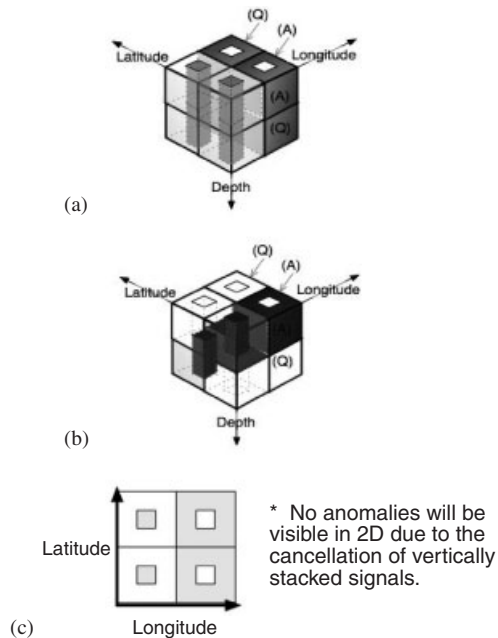


Figure 2. Anomalies to be recovered in a synthetic test model (Figure 1) by 3D or 2D analysis: (a) expected PI anomalies in 3D analysis; (b) expected RI anomalies in 3D analysis; and (c) expected PI and RI anomalies in 2D analysis.

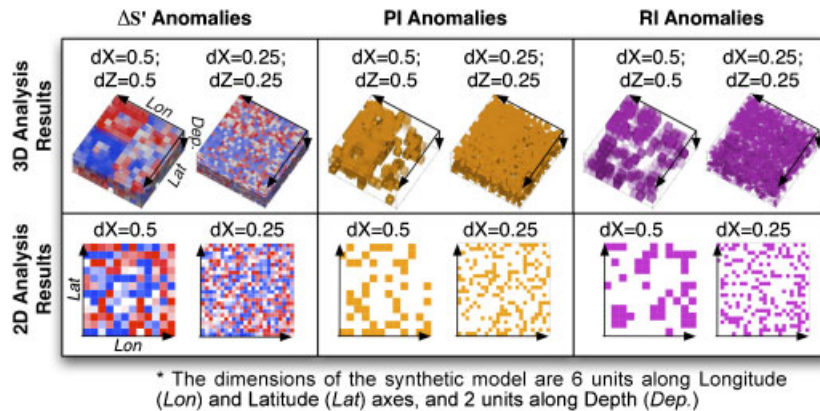


Figure 3. Signal recovery test results on a synthetic model (cf. Figures 1 and 2).

The magnitude of target event to be forecast is often selected to equal: $M \geq M_{\min} + 2$, where M_{\min} is the minimum magnitude of events available in a data set. The magnitude difference value '+2' is based on empirical studies of data quality and availability in an area such as California, but also may be related to the regional earthquake production rate. It is possible to select different values across a range of magnitude units to calibrate the tool for a particular study area or data set. In addition, this may be related to the differences between activation and quiescence behavior, which can be detected with this analysis. For example, one might select for the magnitude difference to be between +1.5 and +3 units (e.g. [30,43–45]) to test a null hypothesis that precursory activation signals related to the long-range power-law-type acceleration do not exist (although the size of acceleration volumes would be far larger than the discretization unit-length applied in this analysis). As for precursory quiescence (e.g. [46]), we would still need to accumulate the appropriate region-specific statistics for future PI analyses. One potential method for determining the optimal set of parameter values for a given study area, again, is to vary the parameters across a range of possible sets of values by means of the grid search technique [cf. 15,16,31,42] with the help of a forecast verification tool (discussed in Section 2.5).

The temporal binning size ' dT ' is selected as one day in our case analyses below, however, the optimal parameter value should be sought, which would be specific to the nature of physical system being investigated. This parameter is important, particularly for the Alternative PI Method (discussed next), in that it is related to the sensitivity of PI forecasting given the presence of significant temporal clustering in data (cf. Sections 3 and 4), and is also related to the overall adherence to the statistical independence assumption of the point process in a study.

The 'Alternative PI Method,' as it appears in our case study, employs 'the counts of days with at least one event' instead of 'daily counts of events' in the representation of activity rate $\psi_{obs}(x_i t)$ (Step 2, Section 2.2). It is essentially a binary measure of seismicity rate. This simple procedure eliminates the potential effects of temporal clustering in shorter than 1 day without perturbing the signals that we seek in the analysis. The difference between the original and this alternative method provides practical information as to the nature of temporal clustering in the data (cf. Section 4). Such information would be very valuable for the future development of

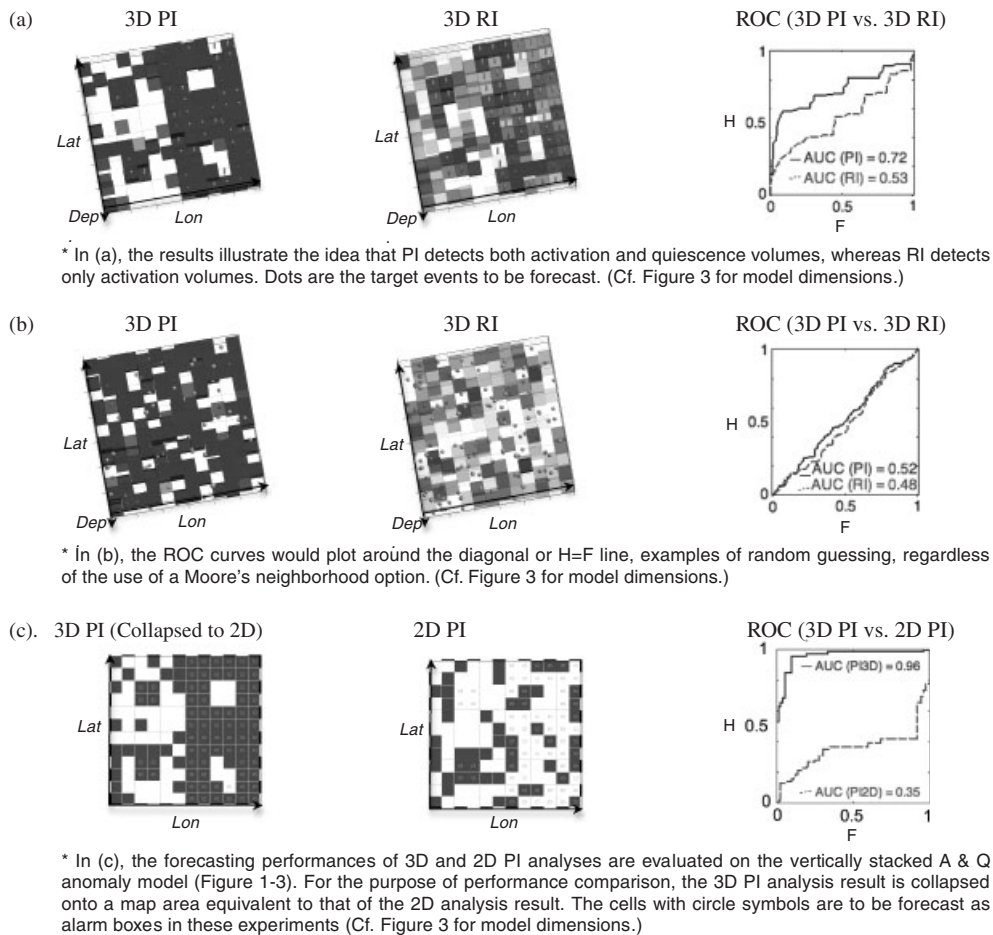


Figure 4. Test comparisons of forecasting performance by various methods: PI or RI; 3D or 2D.

declustering algorithm specific to the PI approach, without the use of additional and arbitrary windowing techniques.

The duration of the 'change time $|t_2 - t_1|$ ' is typically selected to match that of the 'forecasting period $|t_3 - t_2|$ ', based on the hypothesis that the diffusion rates of pre-seismic and post-seismic activities are approximately equal and constant (e.g. [1,2,4]). Alternatively, one might select the time durations based on the statistics of empirical precursor time for a given target magnitude event to be forecast (e.g. Figure 5 in Scholz [47]). At the current stage of this tool development, however, it is more important for one to validate the effective ergodic nature of the system being investigated before selecting the time-intervals. Tiampo *et al.* [16,25,26] and Li *et al.* [15] demonstrated, through practical case studies of both natural and synthetic seismicity data, the importance of effective ergodicity for the optimal performance of PI forecasting. We



Table II. The PI terminologies.

t_0 :	The beginning (inclusive) time of an earthquake catalog
t_1 :	The beginning (inclusive) of the 'change time'
t_2 :	The end (exclusive) of the 'change time', or the beginning (inclusive) of the forecasting period
t_3 :	The end (exclusive) of the forecasting period
$\Delta S'$ anomalies	Anomalous +/- activity rates with respect to the regional mean rate (e.g. [10])
PI anomalies	Volumes in anomalous seismic activity (both activation and quiescence)
RI anomalies	Relative Intensity (RI) is defined as in article [12], and is based on the hypothesis that precursory anomalies are associated with long-term clustering of seismicity (time between t_0 and t_2)

find that many natural fault systems behave effectively ergodic but occasionally punctuated by large earthquake occurrences, where abrupt breaks are found in the linearity of inverse TM curves, and that PI forecasts that take this into consideration perform better than the PI forecasts that do not.

2.4. Forecasting source dimension, geometry, and mechanism

Stress/strain accumulation occurs in all three spatial dimensions. It is essential to analyze seismic activities in 3D, where practicable, in order to accurately assess source dimensions, geometries, and mechanisms associated with seismogenic processes. In a situation where activation and quiescence volumes are vertically stacked, for example, 3D analysis is a necessary option to correctly resolve the vertical profile of such anomalies. The following experiment (Figures 1–4) demonstrates the importance of a 3D analysis in this regard by evaluating the PI's performance in resolving controlled seismic activation and quiescence volumes utilizing a synthetic catalog (with perturbations added at known instances to a uniformly randomized catalog). In addition, the inherent property of the PI approach compared with that of a benchmark 'Relative Intensity (RI)' [12] alternative is also illustrated through this experiment.

In this experiment, a synthetic catalog with white noise is perturbed systematically to give abrupt rate changes in the mid-term (indicated as ' t_1 ' in Figure 1(a)) of the data set, arranged in a particular manner in space as shown in Figure 1(b). The study volume is essentially partitioned into two sets of subvolumes: activation volumes (A) (in red color) and quiescence volumes (Q) (in blue color). Only activation volumes are expected to be identified as RI anomalies, as RI is a measure of long-term ($|t_2 - t_0|$) 'spatial' relative intensity of seismic activity in a study area, as defined in Holliday *et al.* [12], while the PI would detect both types of anomalies: A and Q.

In a 3D analysis, both anomalous volumes stacked vertically would be recoverable, provided that the anomalous signals are strong enough with respect to the background noise. On the contrary, the vertically overlapped signals with the opposite sense (activation vs quiescence) would be invisible in a 2D analysis, and only random noises would remain, Figures 1–4. In addition, as can be seen in Figure 4(a), the PI is capable of resolving both intermediate-term activation and quiescence anomalies, while RI responds only to long-term relative activation anomalies.

The above experiment suggests that certain selections of mapping parameters can influence the apparent recovery rate of the modeled anomalies, provided that target anomaly sizes are known.



However, the apparent drop in the recovery rate of expected anomalies in the above example (Cases for $dX = 0.25$ and $dZ = 0.25$, Figure 3) is likely due to the oversampling of artificially uniform random noise in the background. The presence of signals hidden beneath such spurious noises can be elucidated by the application of a receiver operating characteristic (ROC) test with a Moore neighborhood option (cf. Section 2.5, below). In addition, the above experiment illuminates the fact that the superior forecasting power of PI with respect to RI follows from the PI's ability to detect precursory seismic quiescence signals. RI does not detect any quiescence signals (Figures 1–4).

2.5. Forecast verification and skill evaluation

An ROC diagram [27] is utilized to evaluate the PI's performance in binary forecasting of moderate magnitude events. (ROC analyses are routinely applied in weather forecasting and in medical diagnosis, etc., and are based on the signal detection theory.) The combined use of ROC diagrams and synthetic models such as shown earlier in Figures 1–4 also can help in the assessment of the overall improvement of a modified PI method in forecasting skill with respect to that of the original method (e.g. Figure 4(c)). Similar applications of ROC diagram are found in studies by Holliday *et al.* [12–16,28–30], for the assessment of PI's performance with respect to that of RI alternatives (e.g. Figure 4(a)) or random guesses (e.g. Figure 4(b)).

The criteria employed in the ROC analyses of moderate magnitude event forecasts are as follows. For the performance measure of forecasting target events occurred between time ' t_2 ' and ' $t_2 + |t_2 - t_1|$ ', we define **a** = *a* hit, where an event occurred in a 'hotspot' or an alarm box; **b** = *a* false alarm, where no event occurred in a hotspot; **c** = *a* miss, where an event occurred in a white (non-hotspot) box; **d** = *a* correct rejection, where no event occurred in a white (non-hotspot) box; **n**(the total number of test cases) = **a** + **b** + **c** + **d**. In ROC analyses, **H**(hit rate) is defined as: **H** = **a**/(**a** + **c**), and **F**(false alarm rate) is defined as: **F** = **b**/(**b** + **d**). In general, ROC curves for more skillful forecasting would plot further away from the no-skill line (the diagonal or **H** = **F**, the case of random guesses). Area Under the Curve (AUC) is used as a measure to describing the relative performance of forecasts. AUC ranges from 0 to 1, where AUC of 0.5 would be equivalent to a random guessing and AUC of 1 would mean the forecast to be perfect.

Each different earthquake catalog contains events recorded under various observational conditions, e.g. different station coverages, etc. and accordingly, variations exist in precision of event locations. In order to account for such potential location errors, we often consider events that fall within a Moore's neighborhood around a hotspot toward the statistics, for example [12] (cf. Case analyses, Section 3, below). However, the Moore's neighborhood option is not applied for these ROC analyses on synthetic models shown in Figure 4(a) and (c).

3. CASE ANALYSES

This section provides case study results of retrospective PI analyses performed on natural earthquake data from three seismically active regions: (a) regional view of shallow seismic activities in western Canada fault systems including the Queen Charlotte triple junction in Section 3.1 [48], (b) Taiwan Island, a locus of highly active and complex collisional tectonics on the western edge of the Pacific

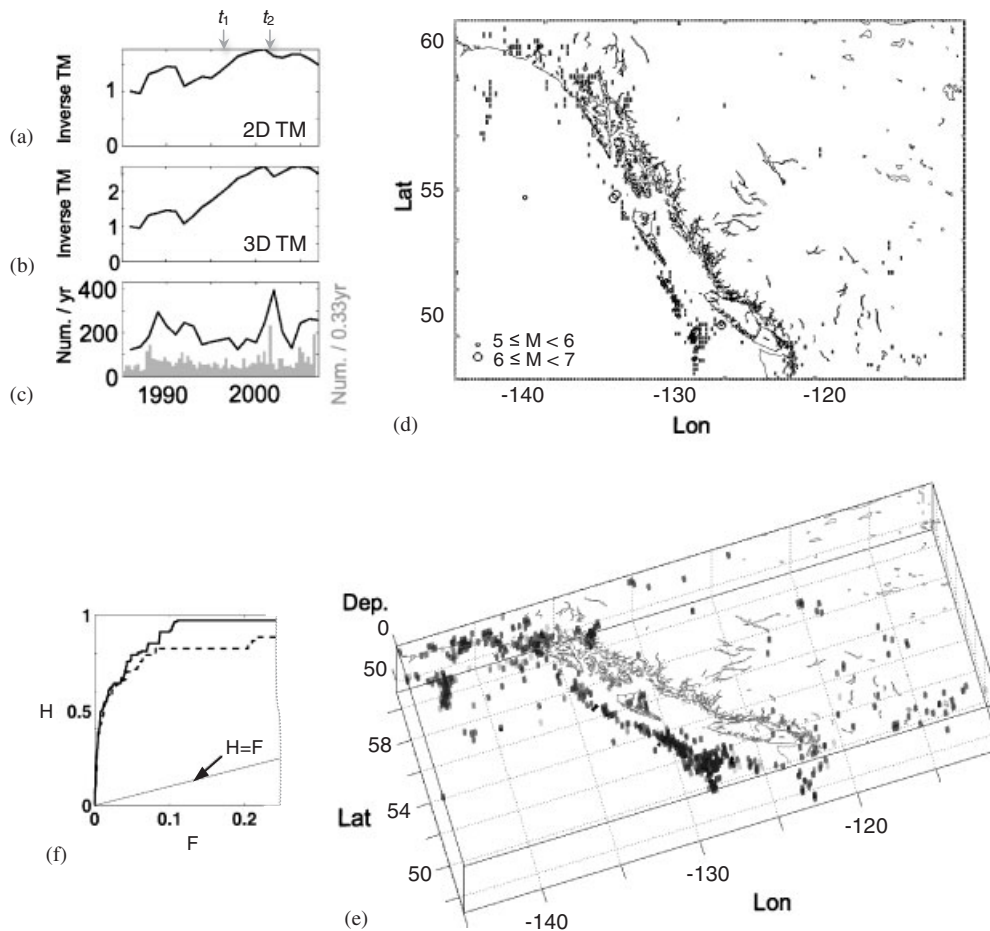


Figure 5. Analysis results for western Canada: (a) 2D TM for $M \geq 3$ seismicity; (b) 3D TM for $M \geq 3$ seismicity; (c) time series of annual seismicity rate for $M \geq 3$; (d) 2D PI analysis result for target magnitude events $M \geq 5$ (circles); (e) 3D PI analysis result for target magnitude events $M \geq 5$ (circles); and (f) ROC diagrams comparing the forecasting performances of 2D PI and 3D PI for target magnitude events $M \geq 5$. Dashed line is for the 2D PI (AUC = 0.93), and solid line is for the 3D PI (AUC = 0.96). The 3D analysis result was collapsed into a 2D map with a map-coverage equivalent to that of the corresponding 2D analysis result before the comparison.

Rim in Section 3.2, and (c) the Java–Sumatra region in Section 3.3, a megathrust subduction zone that has hosted multiple large to great subduction earthquakes in the recorded history. The PI technique's performance in retrospective forecasting of moderate magnitude events is evaluated in cases (3.1) and (3.2), in a similar manner as introduced in Holliday *et al.* (e.g. [12]). In the case study of Section 3.3, we demonstrate one example where PI analyses detect anomalous activities prior to great earthquakes.



3.1. Retrospective forecasting of shallow moderate magnitude seismicity in western Canada

This study area includes the highly seismically active Explorer microplate, about which three plates meet: the Juan de Fuca plate subducts beneath the North American plate (the northern end of the Cascadia subduction zone), the Queen Charlotte transform fault continues to the north, and the Juan de Fuca Ridge meets the others offshore Vancouver Island at the Queen Charlotte triple junction [49,50]. Along the Queen Charlotte transform fault, the largest Canadian earthquake ($M8.1$) occurred in 1949 since the 1700 Cascadia earthquake ($\sim M9$) [50]. For this area, the NRC National Earthquake Database [35] $M \geq 3$ is used for the retrospective forecasting of shallow moderate magnitude seismicity. The following mapping parameters are used: Target Magnitudes of $M \geq 5$ for 3D analysis and $M \geq 4.5$, $M \geq 5$, $M \geq 5.5$ for 2D analysis; $dX = 0.2^\circ$; $dZ = 5$ km; the change time $[t_1, t_2) = [1997/1/1, 2002/1/1)$; and the forecast time $[t_2, t_3) = [2002/1/1, 2007/1/1)$.

Figure 5 shows the TM metric analysis results (Figure 5(a),(b)) and the corresponding seismicity time-series (Figure 5(c)). Identical mapping parameters as applied for the PI analyses (Figure 5(d),(e)) are used in the TM metric analyses. The system under investigation is in general effectively ergodic for most of the training time period $[t_0, t_2)$, except for some disturbances caused by moderate to large earthquake sequences in the area. These selections of the training period and the change time $[t_1, t_2)$ are based on data availability and the effective ergodicity results for this fault system.

Figure 5(f) shows ROC curves comparing the results of the 2D and 3D PI analyses (Figure 5(d),(e)). For the purpose of comparison, the 3D analysis result was collapsed into a 2D map with a map-coverage equivalent to that of the corresponding 2D analysis result (as demonstrated in Figure 4(c)). ROC curve representing the performance of the 3D forecasting plots much further away from the no-skill line than that of the 2D analysis, demonstrating the better forecasting performance of a 3D over a 2D approach.

The results summarized in Table III suggest that the optimal forecasting performance of 2D PI is possible for target magnitude events $M \geq 5$ in this study area. Furthermore, the 'Alternative PI method,' which discounts potential effects from temporal clustering shorter than a day, appears to work efficiently in characterizing anomalous shallow seismicity patterns in the area. Earthquake production rates (per volume [km^3], per time-interval [year]) in this study area are: $9.1e - 7$ for $M \geq 3$ and $2.8e - 8$ for $M \geq 5$.

Table III. Comparison of 2D PI forecasting performance (in AUC*) for various target magnitudes (Study area: Western Canada).

Target magnitude	Alternative PI method		Original PI method	
	w/o Moore	w/Moore	w/o Moore	w/Moore
M 4.5	0.83	0.93	0.8	0.9
M 5.0	0.88	0.96	0.81	0.92
M 5.5	0.72	0.93	0.67	0.88

Suggested target magnitude and the corresponding AUC values are highlighted in boldface.

*AUC = Area under the curve of ROC.



3.2. Retrospective forecasting of moderate magnitude earthquakes in Taiwan region

Taiwan Island is situated above a subduction-collision complex, where the Philippine Sea plate obliquely subducts beneath the Ryukyu subduction zone due northwest (~N50W [51]), which collides against the island on the Eurasian continent from the east [52]. Also, South China Sea subplate (a part of Eurasian continental shelf) subducts beneath the Phillipine Sea plate eastward in the south of the island [53]. Superposition of multiple collisional forces makes the area highly seismically active at depth, where the shape of the deformed Ryukyu slab can be perceived in the cloud of seismicity 100 km beneath the island [52]. The earthquake catalog of the CWB in Taiwan is applied for this study. The geographical area covered in this study is from 119.3 to 122.8 in longitude, 21.7 to 25.7 in latitude, with the depth range: 0–30 km (also tried 0–60, 0–100 km), and $M_{\min} = 3$. Mapping parameters for this region are: Target Magnitude ≥ 5 (or various others experimented; cf. Tables IV and V); $dX = 0.1^\circ$; $dZ = 5$ km (also tried 10 km); and the change time $[t_1, t_2) = 1991/1/1-1999/1/1$.

Table IV. Comparison of 2D PI forecasting performance (in AUC*) for various target magnitudes (Study area: Taiwan region). Table information corresponds to Figure 6(c) and (f).

Target magnitude	Alternative PI method		Original PI method	
	w/o Moore	w/Moore	w/o Moore	w/Moore
M 5.0	0.56	0.71	0.52	0.65
M 5.5	0.6	0.77	0.52	0.69
M 6.0	0.65	0.83	0.53	0.76
M 6.5	0.52	0.74	0.44	0.64

Suggested target magnitude and the corresponding AUC values are highlighted in boldface.

Table V. Comparison of 2D PI forecasting performance (in AUC*) for various target magnitudes and depth ranges (Study area: Taiwan region; Base-year= $[t_0, t_1)^\dagger$).

Depth range (km)	Target	Alternative method		Original method	
	Magnitude	w/o Moore	w/Moore	w/o Moore	w/Moore
0–25	M 5.0	0.55	0.7	0.5	0.62
	M 5.5	0.62	0.84	0.51	0.73
	M 6.0	0.64	0.85	0.5	0.71
	M 6.5	0.49	0.83	0.37	0.61
25–50	M 5.0	0.58	0.76	0.54	0.76
	M 5.5	0.82	0.86	0.82	0.89
50–75	M 5.0	0.85	0.92	0.85	0.93
75–100	M 5.0	0.87	0.92	0.87	0.92

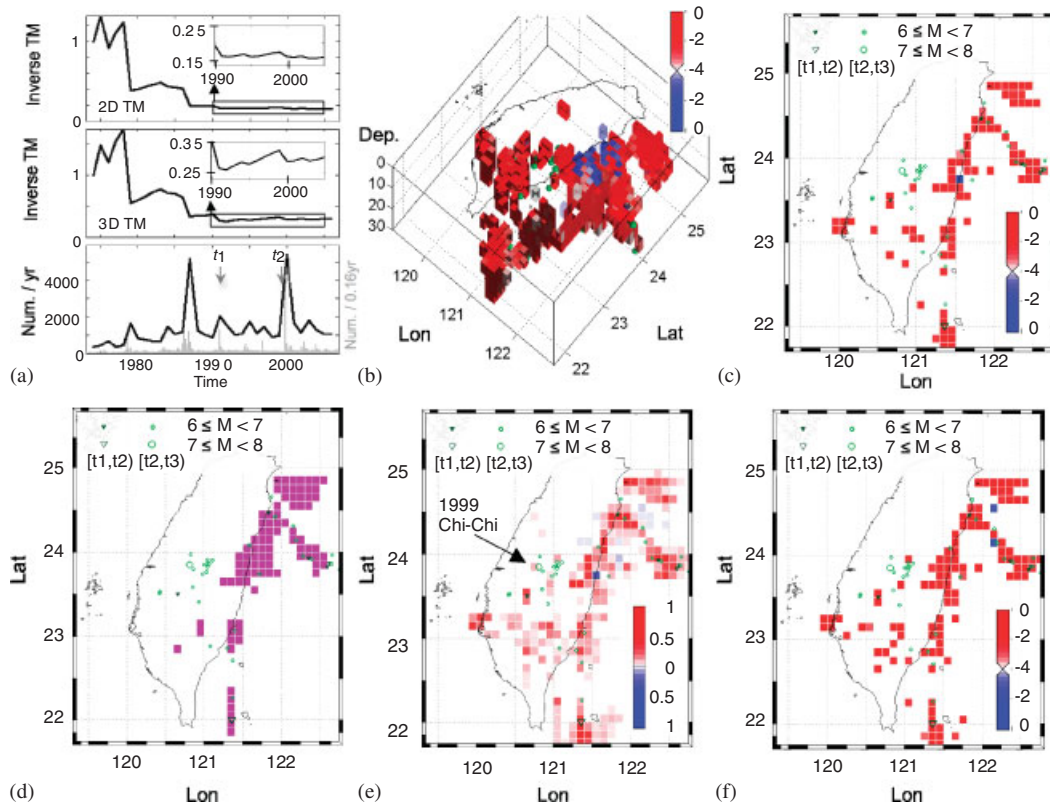
Suggested target magnitude for each depth range and the corresponding AUC values are highlighted in boldface.

*AUC = Area under the curve of ROC.

† Changing the range of base-year shift from $[t_0, t_2)$ to $[t_0, t_1)$ does not affect the statistics.



Figure 6(a) shows the results of TM metric analyses performed with the identical mapping range and parameters as used in the PI analyses in the study area. Shown at the bottom of Figure 6(a) is the annual rate of seismicity ($M_{\min} \geq 3$) for the Taiwan region. Linearity on the inverse TM metric curve for 3D analysis appears to be more pronounced than that of the 2D analysis result. This observation is comparable with the analysis results by Li *et al.* [15] and Tiampo *et al.* [16]. Both 3D and 2D TM metric analysis results suggest that the effective ergodicity of the system is punctuated by multiple large earthquakes, one of which occurs in 1994 [15,16], but for this case study the record segment with this small break in effective ergodicity is intentionally kept within the change time in order to illustrate the robustness of the PI method. Ensemble size selected here is



- Light green-color dots are the target events $M \geq 6$ to be forecast.
- For (b), (c) and (f), activation blocks are shown in red and quiescence blocks in blue, in \log_{10} scale [e.g., 30].
- For (e), $\Delta S'$ values are shown in linear scale, activation blocks in red and quiescence blocks in blue.

Figure 6. Analysis results for Taiwan region: (a) TM curves and annual seismicity rate for $M \geq 3$; (b) 3D PI analysis result for target magnitude events $M \geq 6$ (original method); (c) 2D PI analysis result for target events $M \geq 6$ (original method); (d) 2D RI analysis result for target events $M \geq 6$ (original method); (e) 2D $\Delta S'$ analysis result for target events $M \geq 6$ (original method); and (f) 2D PI analysis result for target events $M \geq 6$ (alternative method).



slightly smaller than that of the analysis performed by Li *et al.* [15] for the same objective. Annual earthquake production rates (per volume [km^3], per year) in this study area are: $2.8e-4$ for $M \geq 3$ and $3.8e-6$ for $M \geq 5$. In comparison with the annual earthquake production rates of western Canada case study area (Section 3.1), this study area is roughly 310 for $M \geq 3$ and 140 for $M \geq 5$ times more active.

Apparent quiescence volumes at shallow depths can be identified in the 3D PI analysis result (Figure 6(b)). Even when the dZ value is changed to 10 km or when the analysis depth range is changed from 0–30 to 0–60 or 0–100 km, the apparent quiescence volumes can still be identified. On the other hand, the quiescence volumes are not visible in the 2D analysis result (Figure 6(c)). Also, there are a few hotspots visible near the epicenter of the 1999 Chi-Chi earthquake in the 3D analysis result, while they are not visible in the 2D analysis result.

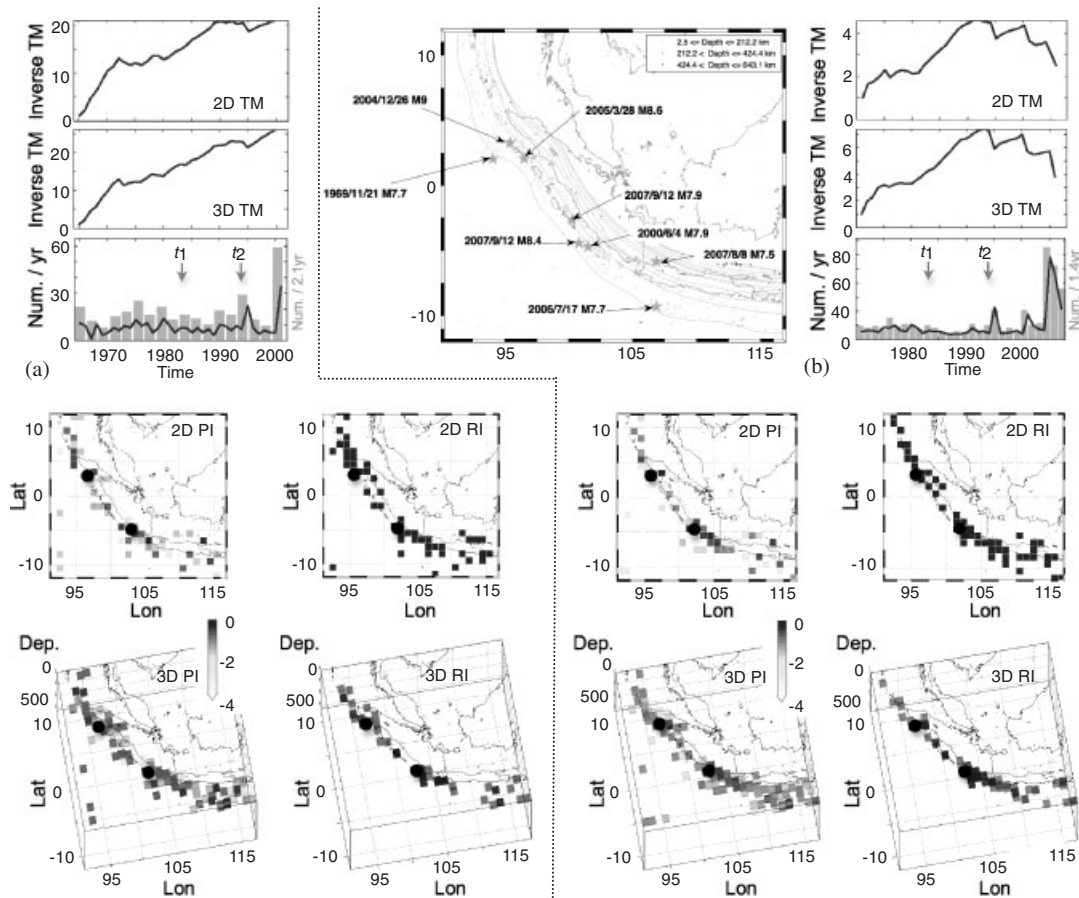
PI anomalies or hotspots (Figure 6(c)) are more spread out than those of RI anomalies (Figure 6(d)), although the hotspots around the 1999 Chi-Chi earthquake are not visible in the 2D PI analysis result of the original method with this particular (not optimal) set of observational parameters (Figure 6(c)). In contrast, RI anomalies highlight only areas that have relatively high seismic activity for the long time period that of $[t_0, t_2)$, e.g. Figure 6(d).

As can be seen in Figure 6(e) of $\Delta S'$ anomalies, where we would find the drifts of state vectors, we can recognize that there were some activities near the imminent 1999 Chi-Chi earthquake sequence. In an alternative view of the same system, when a small degree of temporal clustering treatment is performed (Alternative PI Method, Figure 6(f)), some hotspots around the Chi-Chi earthquake sequence become visible. Target magnitude for the optimal 2D PI forecasting in this particular study area is suggested to be around 6.0, as summarized in Table IV. The Alternative PI Method appears to perform well for this particular study setting also.

In general, PI (2D) forecasting appears to perform better with depth, and at the same time, the difference between the performance of the Alternative PI Method and the Original PI Method becomes small with depth (Table V).

3.3. Retrospective forecasting of imminent great earthquake rupture areas in Java–Sumatra region

The 2004 Sumatra (Indian Ocean) Earthquake Sequence was the fourth largest instrumentally recorded earthquake to occur since 1900 [54]. The earthquake occurred along a ~ 1000 km stretch of the northern Sumatra subduction zone, which was sparsely covered by seismological observation networks at the time of the event occurrence. In this case study, we apply the PI method to two independent sets of catalogs: (1) Centennial Earthquake Catalog and (2) ANSS Catalog for the same geographical area, in order to see the coherence [21] of PI analysis results. Map ranges are: longitude: 91 to 117; latitude: -12 to 12, the depth range: 0 to 650 km, and the same magnitude range $M \geq 5.5$. Owing to the limited availability of data particularly in time, however, unequal durations of the catalogs were employed in the analyses (1964–2002 for Centennial Catalog; 1970–2007 for ANSS Catalog). Mapping parameters used for this region are: Target Magnitude ≥ 7.5 , $dX = 1^\circ$, $dZ = 25$ km (Changing dZ value to 50 km, for example, does not change the results significantly), and the change time is set for $[t_1, t_2)$: 1983/1/1–1994/1/1. Here, we apply the PI method to forecast the potential areas of stress accumulation before great target magnitude events.



- Dot symbols indicate seismicity $M \geq 7.5$ occurred in the time-interval $[t_2, t_3]$, target magnitude events for these forecasting experiments. Clearly, "dots" are insufficient in characterizing the megathrust rupture processes. However, the analysis results commonly illustrated a case where large earthquakes occurred in areas with high precursory seismic activity.
- Map projection code for 2D analysis result displays [55]
- Source of contours for the Sumatra subduction slab [56]

Figure 7. Analysis results for Java–Sumatra region: (a) Centennial catalog ($M \geq 5.5$) and (b) ANSS catalog ($M \geq 5.5$).

Figure 7 summarizes the analysis results for Java–Sumatra region (On the left, Figure 7(a), the results from using the Centennial Earthquake Catalog are shown, and on the right, Figure 7(b), the results from using ANSS Catalog are shown.) From the top of the figure, displayed are: 2D and 3D TM metric analysis results using the same mapping parameters as those for the PI analyses, the time series of annual $M \geq 3$ seismicity rate from the corresponding data set, and followed by the 2D/3D and PI/RI analysis results.

Large kinks on a TM curve are due to sudden changes in the energy of the system, due to detection level changes or large earthquakes with numerous aftershocks [16,25,26]. Both catalogs



are behaving in piecewise effectively ergodic manner up until 1994, when two $M \geq 7.5$ shallow earthquakes occurred in the analysis area (in 1994 and 2000) before the 2004 Sumatra earthquake.

PI and RI analysis results from using different catalogs: Centennial and ANSS, overall look the same in either set. What is striking is that the apparent stress accumulation volumes contain the imminent rupture surfaces of great earthquakes to be forecast, found in either set of the results (cf. Figure 7). The PI method is a good proxy for stress changes (e.g. [10]). As earthquake rupture occurs over a large region, not a single point, we would need an alternative forecast verification scheme that takes into account this discrepancy, particularly for these large target events ($M \geq 7.5$, as in this case).

4. DISCUSSION

Analysis results above illustrate that the Pattern Informatics (PI) approach is applicable in 3D, and support the hypothesis that there is a consistent improvement of PI forecasting performance in 3D over 2D analysis. The results of retrospective analyses (retrospective forecasting of moderate magnitude events) also demonstrate that the 3D PI approach is particularly advantageous in detecting vertically overlapped seismicity anomalies. Moreover, results support the idea that the forecasting performance would improve when the analyses were carried out on an effectively ergodic system [16].

Case studies (Sections 3.1 and 3.2) demonstrate typical examples of PI forecasting for moderate magnitude events. The forecast performances were excellent for example Section 3.1 even without the application of a Moore neighborhood option to account for event location errors, whereas for the case in Section 3.2, alternative treatments were necessary. Notable differences between the two case analyses include ensemble size and earthquake production rate.

In view of PI index calculation, effective ergodicity of a system can appear different (Figure 8). Figure 8 shows the inverse TM metric curves of a point process being observed, while the state vectors for $[t_0, t_1)$ and $[t_0, t_2)$ are calculated as in Steps 3–5, Section 2.2. Uniform random process would be viewed as effectively ergodic in both sweeps with the base-year shift (Step 5, Section 2.2): ‘TM1’ and ‘TM2’ (as in Figure 8(a)). An earthquake sequence with numerous aftershocks in the change time $[t_1, t_2)$ would cause the effective ergodicity of the process to be punctuated as shown in an extreme example, Figure 8(b). In view of the state vector calculation in TM2, the rate at which the phase space is explored is significantly altered in appearance. When temporal clustering shorter than one day is eliminated, as in the Alternative PI Method, the rate at which the phase space is explored is mostly restored as it should be, Figure 8(c). In this manner, we can make further improvements to the current PI approach.

4.1. 3D vs 2D PI forecasting performance

Apparent quiescence volumes identified in the 3D PI analysis result for Taiwan region (Figure 6(b)) are not visible in the 2D analysis (Figure 6(c)). The reason for the latter is at least partly due to the cancelation of vertically stacked anomalies in the opposite sense (shallow quiescence volumes vs deep activation volumes), as demonstrated in Figures 1–4 using a synthetic model. A 3D analysis clearly provides more information about the system being investigated (in depth), hence allowing

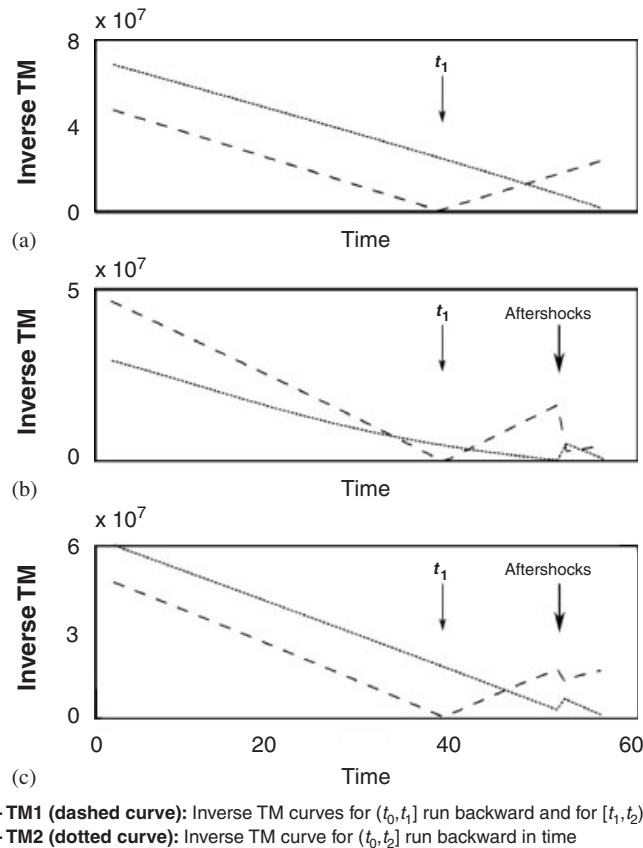


Figure 8. Effective ergodicity in view of the PI index calculation, on synthetic catalog: (a) effective ergodicity in view of the PI index calculation on uniform random process; (b) effective ergodicity in view of the PI index calculation on uniform random process with an aftershock sequence in the change time $[t_1, t_2]$; and (c) effective ergodicity in view of the alternative PI index calculation (Alternative PI Method) on uniform random process with an aftershock sequence in the change time $[t_1, t_2]$.

an improvement in forecasting performance. For the purpose of performance comparisons using ROC diagrams, 3D PI analysis results were collapsed into a 2D map area equivalent to that of the corresponding 2D analysis results (e.g. Figure 4(c)). 3D PI forecasting apparently outperforms a 2D PI analysis. 3D PI analysis is particularly advantageous over 2D analysis in resolving vertically overlapped seismicity anomalies in a highly complex tectonic environment such as Taiwan region.

4.2. Ensemble size vs forecasting performance

Correlation is found between the forecasting performance and the ensemble size for PI analyses, although such correlation does not exist in analyses of ideally uniform random synthetic data. The correlation likely comes from the facts that seismicity tends to occur in confined areas along



preexisting weaknesses in the crust, particularly near plate boundaries, and that the proportion of relatively inactive cells would increase rapidly with increasing ensemble size in a natural fault system. Ensemble size can be adjusted by altering the applicable study volume (map ranges in longitude, latitude, and depth) or by varying the binning units (dX or dZ). As long as the earthquake data set in a study area is homogeneous (and ideally complete,) making adjustments to the ensemble size would be a valid procedure to optimize the PI's forecasting performance. As the ensemble size is increased, the representativeness of statistical ensembles utilized in the PI or TM calculation improves, or the robustness of PI forecasting performance would enhance, even with the presence of large earthquake sequences in the record. This is in accord with the observations made by Tiampo *et al* [16], in that the use of appropriate spatial, temporal, and magnitude parameter ranges for ergodic behavior of the system in a study ensures that the spatial and temporal averages are stationary, resulting in better performance of the PI method.

4.3. Event depths vs forecasting performance

Aside from the technical aspects of performance improvements in moderate magnitude event forecasting, there appears to exist a natural condition where (2D) PI forecasting performance systematically becomes 'influenced' somehow, possibly due to dissimilarities in conditions (such as pressure, temperature, and structure/geometry) and materials. In Table V (Taiwan case), we saw that PI's performance improved with depth, while at the same time, the difference between the performance of the Alternative PI Method and the Original PI Method became very small with depth. This set of observations supports the idea that intermediate depth seismicity is often accompanied by fewer dependent events compared with shallower mainshocks of the equivalent magnitudes [57], and in that sense the seismicity at depths is comparatively less clustered through a natural mechanism. Furthermore, the results demonstrated that the gradual improvement of detection level in depth in earlier records and the default depths (5 or 10 km) assigned for inadequately located events (e.g. Section 3.2; Taiwan case) had negligible effects on the PI's performance.

4.4. PI vs RI

PI method characterizes spatio-temporal changes in seismicity rate, which is a good proxy for stress changes, Tiampo *et al.* (e.g. [10]). As can be seen in Figures 7(a) and (b), regardless of the difference in the catalog sources: Centennial or ANSS, stress accumulation is apparent in large volumes that contain imminent rupture surfaces (cf. [58–60]). As earthquake rupture occurs over a region and is not a single point, we would need an alternative forecast verification scheme, particularly for these large target events ($M \geq 7.5$ as in this case example, Section 3.3). Similarly, the time window employed in these case analyses is too short to compare the forecasting performance between PI and RI. Both methods detect significant amount of activation prior to great earthquakes, denoted as spherical dots in the example maps.

Holliday *et al.* [28] analyzed the same region for temporal fluctuations in the forecasting skill difference between two measures: the PI and RI, using a Pierce difference function $dA = (PSS_{RI} - PSS_{PI})$, with the understanding that the PI and RI are sensitive to different effects. They found that large to great earthquakes (in California and Sumatra region) tend to follow a period of positive dA values, where RI's performance significantly exceeds that of the PI in relative terms. It would



be interesting to pursue the research on the timing of these dA peak occurrences and the tectonic implications of such observations, as the dA peaks also appear to coincide with ergodicity breaks on inverse TM metric curves.

As seen in Section 2 using the synthetic catalogs, the PI is inherently different from the benchmark RI measurements in its ability to detect both seismic activation and quiescence, while RI only provides long-term relative intensity in seismic activity. Therefore, the occurrence of stress shadows (e.g. [61]) would be detected as short-term to intermediate-term PI anomalies but not as positive RI anomalies.

4.5. Limitation of grid-based binary forecasting for moderate magnitude events

Grid-based binary forecasting experiments e.g. [40] have taken an important step toward the development of reliable earthquake forecasting schemes. Nevertheless, we would need to keep moving ahead for non-grid-based approach, perhaps. Grid-based approach considers an earthquake as a point and is based on the assumption that a target event would occur exactly in a single cellular region with high probability. In order to forecast events of certain magnitudes and greater corresponding to the ones above the scaling break in rupture surface area and magnitude relation [62,63], a different approach for forecast verification might be necessary (e.g. Figure 9). This is beyond the scope of the current study, and will be explored elsewhere.

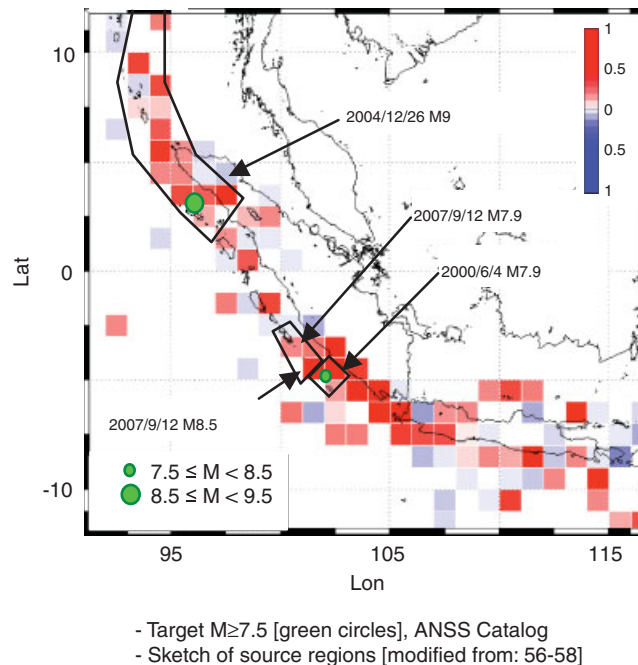


Figure 9. 2DAS' map for Java–Sumatra region.



Effective ergodicity of the system under investigation is one of the key factors in improving the PI application in studies of natural seismicity patterns [16,26]. As seen in the case analysis results (Figure 5, 6, and 7), effectively ergodic periods exist in most natural fault systems investigated, occasionally punctuated by apparent and sudden bursts of energy release as dependent earthquakes following large events [16], which could extend beyond the discretization unit-length of a target magnitude event point process. In addition, nonlinear changes of slope on the inverse TM metric curve might be attributed to a gradual change in the operational condition of a seismic network, and effects of such rate changes are currently investigated by utilizing both synthetic and natural seismicity data. A method is also being developed to minimize the effects from ergodicity breaking processes on PI index calculation. Selecting the optimal set of mapping or observational parameters (e.g. dT value) would help to improve our PI forecasting. These investigations are underway.

5. CONCLUSION

The PI approach is applicable in 3D, and the results of retrospective forecasting of moderate magnitude events demonstrate that 3D PI approach is particularly advantageous in detecting vertically overlapped seismicity anomalies. Results also support the hypothesis that the forecasting performance would further improve when the analyses were carried out on a data set that effectively satisfies the statistical ergodicity and independence requirements of point processes [1–3,16,26]. Calibrating the forecasting tool for each study area with a suitable set of mapping parameters in space, time, and magnitude would also help to improve the PI's forecasting performance. In addition, an alternative forecast verification scheme is necessary, particularly for great earthquake forecasting, which would need to appropriately consider both the geometrical asymmetry of main-shock ruptures and of alarm volumes. Finally, statistics of precursory activity durations, spreads, and magnitudes, in connection with the specific sets of mapping parameters for studies in various tectonic environments would need to be accumulated, which in turn would help to determine the suitable set of observational parameters and for further improvements to the forecasting performance via PI approach.

ACKNOWLEDGEMENTS

We would like to thank the effort of earthquake data sources, to maintain their seismic networks and to compile earthquake catalogs: Centennial Earthquake Catalog [32,33], Advanced National Seismic System (ANSS) Earthquake Catalog in the U.S. [34], Earthquake Catalog by the Central Weather Bureau (CWB) of Taiwan, and National Earthquake Database of Canada [35]. This work was funded by the NSERC and Aon Benfield/ICLR IRC in Earthquake Hazard Assessment, and the Southern California Earthquake Center (SCEC). SCEC is funded by NSF Cooperative Agreement EAR-0529922 and USGS Cooperative Agreement 07HQAG0008. The SCEC contribution number for this paper is 1243.

REFERENCES

1. Tiampo KF, Rundle JB, McGinnis SA, Gross SJ, Klein W. Mean-field threshold systems and phase dynamics: An application to earthquake fault systems. *Europhysics Letters* 2002; **60**(3):481–487.
2. Tiampo KF, Rundle JB, McGinnis SA, Klein W. Pattern dynamics and forecast methods in seismically active regions. *Pure and Applied Geophysics* 2002; **159**:2429–2467.



3. Rundle JB, Klein W, Tiampo KF, Gross SJ. Linear pattern dynamics in nonlinear threshold systems. *Physical Review* 2000; **61**(3):2418–2432.
4. Rundle JB, Tiampo KF, Klein W, Sa' Martins JS. Self-organization in leaky threshold systems: The influence of near-mean field dynamics and its implications for earthquakes, neurobiology, and forecasting. *Proceedings of the National Academy of Sciences* 2002; **99**(suppl. 1):2514–2521. DOI: 10.1073/pnas.012581899.
5. Egolf DA. Equilibrium regained: From nonequilibrium chaos to statistical mechanics. *Science* 2000; **287**:101–104.
6. Rundle JB, Turcotte DL, Shcherbakov R, Klein W, Sammis C. Statistical physics approach to understanding the multiscale dynamics of earthquake fault systems. *Review of Geophysics* 2003; **41**(4). DOI: 10.1029/2003RG000135.
7. Tiampo KF, Rundle JB, McGinnis SA, Gross SJ. Eigenpatterns in southern California seismicity. *Journal of Geophysical Research* 2002; **107**(B12):2354. DOI: 10.1029/2001JB000562.
8. Klein W, Anghel M, Ferguson CD, Rundle JB, Sa' Martins JS. Statistical analysis of a model for earthquake faults with long-range stress transfer. *GeoComplexity and the Physics of Earthquakes (Geophysical Monograph, vol. 120)*. AGU Publications: Washington, DC, 2000; 43–71.
9. Mori H, Kuramoto Y. *Dissipative Structures and Chaos*. Springer: Berlin, 1998.
10. Tiampo KF, Rundle JB, Klein W. Premonitory seismicity changes prior to the Parkfield and Coalinga earthquakes in southern California. *Tectonophysics* 2006; **413**:77–86.
11. Tiampo KF, Rundle JB, Klein W, Holliday JR. Forecasting rupture dimension using the pattern informatics technique. *Tectonophysics* 2006; **424**:367–376.
12. Holliday JR, Nanjo KZ, Tiampo KF, Rundle JB, Turcotte DL. Earthquake forecasting and its verification. *Nonlinear Processes in Geophysics* 2005; **12**:965–977.
13. Nanjo KZ, Rundle JB, Holliday JR, Turcotte DL. Pattern informatics and its application for optimal forecasting of large earthquakes in Japan. *Pure and Applied Geophysics* 2006; **163**:2417–2432.
14. Chen CC, Rundle JB, Holliday JR, Nanjo KZ, Turcotte DL, Li SC, Tiampo KF. The 1999 Chi-Chi, Taiwan, earthquake as a typical example of seismic activation and quiescence. *Geophysical Research Letters* 2005; **32**. DOI: 10.1029/2005GL023991.
15. Li HC, Tiampo KF, Chen CC, Klein W, Rundle JB. A retrospective study of the 1999 Chi-Chi, Taiwan earthquake using a 3-D PI method. *Tectonophysics* 2009; submitted.
16. Tiampo KF, Klein W, Li HC, Mignan A, Toya Y, Kohen-Kadosh SZL, Rundle JB, Chen CC. Ergodicity and earthquake catalogs: Forecast testing and resulting implications. *Pure and Applied Geophysics* 2008; submitted. Special Issue: Seismogenesis and Earthquake Forecasting: The Frank Evison Volume.
17. Habermann RE. Man-made changes of seismicity rates. *Bulletin of Seismological Society of America* 1987; **77**(1):141–159.
18. Matthews MV, Reasenberg P. Comment on Habermann's method for detecting seismicity rate changes. *Journal of Geophysical Research* 1987; **92**(B9):9443–9445.
19. Habermann RE. Precursory seismic quiescence: Past, present, and future. *Pure and Applied Geophysics* 1988; **126**: 279–318.
20. Hasegawa A, Hamaguchi H. The masking effect on magnitude distribution by the successive occurrence of earthquakes. *Geophysics* 1972; **21**:51–60. *Scientific Report*, Tohoku University, Series 5.
21. Habermann RE, Creamer F. Catalog errors and the M8 earthquake prediction algorithm. *Bulletin of Seismological Society of America* 1994; **84**(5):1551–1559.
22. Rydelek PA, Sacks IS. Testing the completeness of earthquake catalogs and the hypothesis of self-similarity. *Nature* 1989; **337**:251–253.
23. Ogata Y, Katsura K. Analysis of temporal and spatial heterogeneity of magnitude frequency distribution inferred from earthquake catalogs. *Geophysical Journal International* 1993; **113**:737–738.
24. Woessner J, Wiemer S. Assessing the quality of earthquake catalogs: Estimating the magnitude of completeness and its uncertainty. *Bulletin of the Seismological Society of America* 2005; **95**:684–698.
25. Tiampo KF, Rundle JB, Klein W, Sa' Martins JS, Ferguson CD. Ergodic dynamics in a natural threshold system. *Physical Review Letters* 2003; **91**:238501.
26. Tiampo KF, Rundle JB, Klein W, Holliday JR, Sa' Martins JS, Ferguson CD. Ergodicity in natural earthquake fault networks. *Physical Review E* 2007; **75**:066107.
27. Jolliffe IT, Stephenson DB. *Forecast Verification: A Practitioner's Guide in Atmospheric Science*. Wiley: New York, 2003.
28. Holliday JR, Rundle JB, Tiampo KF, Turcotte DL. Using earthquake intensities to forecast earthquake occurrence times. *Nonlinear Processes in Geophysics* 2006; **13**:585–593.
29. Chen CC, Rundle JB, Li HC, Holliday JR, Nanjo KZ, Turcotte DL, Tiampo KF. From tornadoes to earth quakes: Forecast verification for binary events applied to the 1999 Chi-Chi, Taiwan, earthquake. *Terrestrial Atmospheric and Oceanic Sciences* 2006; **17**:503–516.
30. Nanjo KZ, Holliday JR, Chen CC, Rundle JB, Turcotte DL. Application of a modified pattern informatics method to forecasting the locations of future large earthquakes in the central Japan. *Tectonophysics* 2006; **424**:351–366.



31. Holliday JR, Rundle JB, Tiampo KF, Klein W, Donnellan A. Systematic procedural and sensitivity analysis of the Pattern Informatics method for forecasting large ($M > 5$) earthquake events in Southern California. *Pure and Applied Geophysics* 2006; **163**:2433–2454. DOI: 10.1007/s00024-006-0131-1.
32. Engdahl ER, Villaseñor A. Global Seismicity: 1900–1999. *International Handbook of Earthquake Engineering Seismology, Part A*, ch. 41. Lee WHK, Kanamori H, Jennings PC, Kisslinger C (eds). Academic Press: New York, 2002; 665–690.
33. Engdahl ER, van der Hilst R, Buland R. Global teleseismic earthquake relocation with improved travel times and procedures for depth determination. *Bulletin of Seismological Society of America* 1998; **88**:722–743.
34. ANSS earthquake catalog. Available at: <http://www.anss.org/> [3 February 2008].
35. Natural Resources Canada. National earthquake database of Canada. Available at: <http://earthquakecanada.nrcan.gc.ca/> [3 April 2008].
36. Thirumalai D, Mountain RD. Ergodic convergence properties of supercooled liquids and glasses. *Physical Review A* 1990; **42**:4574–4587.
37. Ferguson CD, Klein W, Rundle JB. Spinodals, scaling and ergodicity in a threshold model with long-range stress transfer. *Physical Review E* 1999; **60**(2):1359–1373.
38. Dieterich J. A constitutive law for rate of earthquake production and its application to earthquake clustering. *Journal of Geophysical Research* 1994; **99**:2601–2618.
39. Toda S, Stein RS. Response of the San Andreas fault to the 1983 Coalinga–Nunēz earthquakes: An application of interaction-based probabilities for Parkfield. *Journal of Geophysical Research* 2002; **107**(B6):2126. DOI: 10.1029/2001JB000172.
40. Holliday JR, Chen CC, Tiampo KF, Rundle JB, Turcotte DL, Donnellan A. A RELM earthquake forecast based on Pattern Informatics. *Seismological Research Letters* 2007; **78**(1):87–93.
41. Wells DL, Coppersmith KJ. New empirical relationships among magnitude, rupture length, rupture width, rupture area, and surface displacement. *Bulletin of the Seismological Society of America* 1994; **84**(4):974–1002.
42. Shcherbakov R, Turcotte DL, Rundle JB, Tiampo KF, Holliday JR. Forecasting the locations of future large earthquakes: An analysis and verification. *Pure and Applied Geophysics* 2008; submitted. Special Issue: Seismogenesis and Earthquake Forecasting: The Frank Evison Volume.
43. Bufe CG, Varnes DJ. Predictive modeling of the seismic cycle of the greater San Francisco Bay region. *Journal of Geophysical Research* 1993; **98**:9871–9883.
44. Jaumè SC, Sykes LR. Evolving towards a critical point: A review of accelerating seismic moment/energy release prior to large and great earthquakes. *Pure and Applied Geophysics* 1999; **155**:279–306.
45. Papazachos CB, Karakaisis GF, Scordilis EM, Papazachos BC. Global observational properties of the critical earthquake model. *Bulletin of the Seismological Society of America* 2005; **95**:1841–1855.
46. Enescu B, Ito K. Some premonitory phenomena of the 1995 Hyogo-Ken Nanbu (Kobe) earthquake: Seismicity, b-value and fractal dimension. *Tectonophysics* 2001; **338**:297–314.
47. Scholz CH. Mechanisms of seismic quiescences. *Pure and Applied Geophysics* 1988; **126**:701–718.
48. Rohr KMM, Furlong KP. Ephemeral plate tectonics at the Queen Charlotte triple junction. *Geology* 1995; **23**(11):1035–1038.
49. Hyndman RD, Rogers GC, Dragert H, Wang K, Oleskevich D, Henton J, Clague JJ, Adams J, Bobrowsky PT. Giant earthquakes beneath Canada's West coast. Geological Survey of Canada. Available at: <http://cgc.nrcan.gc.ca/geodyn/mega.e.php?p=1> [1 September 2008].
50. Geological Survey of Canada. Seismic zones in Western Canada. Available at: <http://earthquakescanada.nrcan.gc.ca/zones/westcan.e.php> [1 September 2008].
51. Seno T, Stein S, Gripp AE. A model for the motion of the Philippine Sea plate consistent with NUVEL-1 and geological data. *Journal of Geophysical Research* 1993; **98**:17,941–917,948.
52. Chou HC, Kuo BY, Hung SH, Chiao LY, Zhao D, Wu YM. The Taiwan–Ryukyu subduction–collision complex: Folding of a viscoelastic slab and the double seismic zone. *Journal of Geophysical Research* 2006; **111**(B04410). DOI: 10.1029/2005JB003822.
53. Wu YM, Chang CH, Zhao L, Teng TL, Nakamura M. A comprehensive relocation of earthquakes in Taiwan from 1991 to 2005. *Bulletin of the Seismological Society of America* 2008; **98**(3):1471–1481. DOI: 10.1785/0120070166.
54. US Geological Survey. Largest earthquakes in the world since 1900. Available at: http://earthquake.usgs.gov/regional/world/10_largest_world.php [1 September 2008].
55. Pawlowicz R. M_Map: A mapping package for Matlab. Available at: <http://www.eos.ubc.ca/~rich/map.html> [2 October 2007].
56. Gudmundsson O, Sambridge M. A regionalized upper mantle (RUM) seismic model. *Journal of Geophysical Research* 1998; **103**:7121–7136.
57. Kagan YY, Knopoff L. Dependence of seismicity on depth. *Bulletin of the Seismological Society of America* 1980; **70**(5):1811–1822.
58. Lay T, Kanamori H, Ammon CJ, Nettles M, Ward SN, Aster RC, Beck SL, Bilek SL, Brudzinski MR, Butler R, DeShon HR, Ekström G, Satake K, Sipkin S. The great Sumatra–Andaman earthquake of 26 December 2004. *Science* 2005; **308**:1127–1132.



59. Ammon CJ, Ji C, Thio HK, Robinson D, Ni S, Hjorleifsdottir V, Kanamori H, Lay T, Das S, Helmberger D, Ichinose G, Polet J, Wald D. Rupture process of the 2004 Sumatra–Andaman earthquake. *Science* 2005; **308**:1133–1139.
60. US Geological Survey. Two decades of ruptures in the Sumatra–Andaman arcs. Available at: <ftp://hazards.cr.usgs.gov/maps/sigeqs/20070912/ModernRuptures.pdf> [1 October 2008].
61. Tiampo KF, Rundle JB, Klein W. Stress shadows determined from a phase dynamical measure of historic seismicity. *Pure and Applied Geophysics* 2006; **163**:2407–2416. DOI: 10.1007/s00024-006-0134-y.
62. Shimazaki K. Small and large earthquakes: The effects of thickness of the seismogenic layer and the free surface. *Earthquake Source Mechanics*. Das JBS, Scholz CH (eds.) (*AGU Geophysical Monograph*, vol. 37). American Geophysical Union: Washington, DC, 1986; 209–216.
63. Pacheco JF, Scholz CH, Sykes LR. Changes in frequency-size relationship from small to large earthquake. *Nature* 1992; **355**:71–73.